Normal Perceptual Sensitivity Arising From Weakly Reflective Cone Photoreceptors

Kady S. Bruce,[1] Wolf M. Harmening,[2] Bradley R. Langston,[3] William S. Tuten,[4] Austin Roorda,[4] and Lawrence C. Sincich[1]

[1]Department of Vision Sciences, University of Alabama at Birmingham, Birmingham, Alabama, United States
[2]Department of Ophthalmology, University of Bonn, Bonn, Germany
[3]School of Medicine, University of Alabama at Birmingham, Birmingham, Alabama, United States
[4]School of Optometry, Vision Science Graduate Group, University of California at Berkeley, Berkeley, California, United States

Correspondence: Lawrence C. Sincich, Department of Vision Sciences, University of Alabama at Birmingham, WORB 638, 1720 2nd Avenue South, Birmingham, AL 35294-4390, USA;
sincich@uab.edu.

Submitted: January 26, 2015
Accepted: April 22, 2015

Citation: Bruce KS, Harmening WM, Langston BR, Tuten WS, Roorda A, Sincich LC. Normal perceptual sensitivity arising from weakly reflective cone photoreceptors. *Invest Ophthalmol Vis Sci*. 2015;56:4431–4438. DOI:10.1167/iovs.15-16547

Purpose. To determine the light sensitivity of poorly reflective cones observed in retinas of normal subjects, and to establish a relationship between cone reflectivity and perceptual threshold.

Methods. Five subjects (four male, one female) with normal vision were imaged longitudinally (7–26 imaging sessions, representing 82–896 days) using adaptive optics scanning laser ophthalmoscopy (AOSLO) to monitor cone reflectance. Ten cones with unusually low reflectivity, as well as 10 normally reflective cones serving as controls, were targeted for perceptual testing. Cone-sized stimuli were delivered to the targeted cones and luminance increment thresholds were quantified. Thresholds were measured three to five times per session for each cone in the 10 pairs, all located 2.2 to 3.3° from the center of gaze.

Results. Compared with other cones in the same retinal area, three of 10 monitored dark cones were persistently poorly reflective, while seven occasionally manifested normal reflectance. Tested psychophysically, all 10 dark cones had thresholds comparable with those from normally reflecting cones measured concurrently ($P = 0.49$). The variation observed in dark cone thresholds also matched the wide variation seen in a large population ($n = 56$ cone pairs, six subjects) of normal cones; in the latter, no correlation was found between cone reflectivity and threshold ($P = 0.0502$).

Conclusions. Low cone reflectance cannot be used as a reliable indicator of cone sensitivity to light in normal retinas. To improve assessment of early retinal pathology, other diagnostic criteria should be employed along with imaging and cone-based microperimetry.

Keywords: adaptive optics, cone sensitivity, retinal imaging

Adaptive optics scanning laser ophthalmoscopy (AOSLO) has provided valuable insight about retinal structure at the cellular level in many diseases. Consequently, clinical interest in using AOSLO imaging to examine disease is likely to continue growing.[1] Although AOSLO has been employed to image numerous retinal structures, it is most commonly used to visualize cone photoreceptors because of their intrinsic ability to reflect incoming light.[2] In retinal disease, cones may be dysmorphic, atrophied, or missing from the mosaic. These factors will contribute to poor reflectance and possibly increased cone spacing in AOSLO images, both of which are metrics commonly used to gauge disease progression. For instance, patients with type 1 diabetes, glaucoma, and Stargardt disease all showed a decrease of cone density,[3–5] while patients with acute macular retinopathy and severe head trauma showed a reduction in cone reflectivity.[6,7] These retinopathies represent a small sample of the potential diseases that may cause cone photoreceptors to appear abnormal in adaptive optics imaging.[8–20] Consequently, it is important to establish how cone reflectivity is related to functional light sensitivity.

The intrinsic waveguiding properties of cones are well established,[21] and depend upon the normally cylindrical shape of the inner and outer segments. If retinal diseases cause either of the segments to become atrophic or dysmorphic, the cones are likely to appear dark within an AOSLO image. However, in normal retinas, it has been reported that there are occasional cones that exhibit unusually low reflectance.[22–24] These cones appear as a dark space within an otherwise regular mosaic, much in the same way that a diseased cone might. It is important to realize that in all subjects imaged with AOSLO, regardless of disease state, cone reflectivity in AOSLO images varies considerably from moment to moment, as well as from day to day. This variation in reflectivity is not completely understood and may arise from multiple factors, including natural morphological variation within cells, refractive index changes associated with photocurrent dynamics, and the coherence properties of the imaging light.[22,25–27] Consistent with the earlier reports, we have observed cones within AOSLO images that exhibit low reflectivity in the perifoveal region. Given that these poorly reflective cones exist in pathological and nonpathological states, this raises the question of whether persistently dark cones in normal subjects represent dysfunctional photoreceptors. If so, dark cones may serve as a useful harbinger of retinal disease at the earliest stages.

Here we sought to determine the light sensitivity of persistently dark cones found in the retinas of normal subjects.

To do so, selected dark cones were first imaged longitudinally using an AOSLO system in a laboratory setting, in order to see how the reflectivity of the cones changed over time scales longer than a single imaging session. Second, the dark cones were targeted for psychophysical testing, where a cone-sized stimulus was delivered to selected cones in the retinal mosaic and increment thresholds were determined.[28] Finally, we examined whether there was any relationship between cone reflectivity and the perceptual thresholds measured with such microstimulation.

Methods

Our multisite, experimental cohort study was approved prospectively by the institutional review boards of the University of Alabama at Birmingham (UAB) and the University of California, Berkeley (UCB), and conformed to the tenets of the Declaration of Helsinki. Written, informed consent was required by all subjects to participate in the research. All participating subjects had 20/20 or better best corrected visual acuity, clear optics, and had normal color vision. Exclusion criteria included highly irregular corneal shape and visual acuity that could not be optically compensated; however, no prospective subjects were excluded.

Retinal Imaging

Cones were imaged using multiwavelength AOSLOs (UAB and UCB) with infrared light (842 ± 25 nm). In each system, the light source was a supercontinuum laser (SuperK Extreme; NKT Photonics, Birkerød, Denmark) bandpass filtered to provide the infrared imaging light and the visible stimulation light (543 ± 11 nm) in separate imaging channels. The rationale for choosing 543 nm for the stimulation wavelength was to minimize the sensitivity differences between the long and medium wavelength sensitive cones. For imaging, specific details pertaining to AOSLO systems have been described elsewhere.[27,29,30] Briefly, light in both channels was projected into the eye via vertical and horizontal scanning mirrors. Infrared light reflected back through the optical system was sampled by a Shack-Hartmann wavefront sensor for measurement of wavefront aberrations. The aberrated wavefront in both light channels was then compensated using a microelectromechanical systems deformable mirror (Boston Micromachines, Cambridge, MA, USA), with the wavefront being continuously corrected in a closed loop operating at 16 Hz.

Single Cone Microstimulation With AOSLO

Microstimulation involves delivering a cone-sized stimulus onto a single targeted cone. Comprehensive methods have been recently described elsewhere.[28] For the present experiments, we used a 5 × 5 pixel square (35 arcsec, ~3.6 μm) of 543-nm light, flashed for a duration of ~130 μs on a constant background of ~4.3 cd/m^2. Taking into account the point spread function of the eye's optics under these imaging conditions, and the small scatter in stimulus delivery,[28] this stimulus size (at the 5% intensity contour) subtended less than 8 μm on the retina (less than 2 arcmin for a typical human eye assuming 290 μm/deg[31]), closely matching the inner segment diameter of the cones at the eccentricities studied (2.2–3.3°).[32] This eccentricity range is optimal for microstimulation because the cone spacing is large enough to be minimally affected by positional delivery errors, yet the sites were within the ~5° limit where such stimuli presented through this system can be seen.[28] Because the imaging and stimulation were performed with different wavelengths, transverse chromatic aberrations were both measured and corrected in each subject.[30] This measurement was made before and after each experiment, to assess whether any lateral shift in the stimulus occurred during the experiment. If measured offsets drifted by more than one half cone width, the data were discarded. Fixational eye movements present in all subjects were compensated for using real-time eye tracking,[33] allowing retinally stabilized stimulus delivery with cumulative delivery errors of less than a cone diameter.[28]

Psychophysical Experiments

Pupils were dilated with 1% tropicamide. Bite bars custom fitted for each subject were used to minimize pupil motion. Retinal locations being imaged were selected by having the subject fixate on a light-emitting diode positioned outside of a 1.2° imaging field. Following transverse chromatic aberration measurement and 15-minute dark adaptation, the psychophysical experiments commenced self-paced. Subjects used a keyboard to initiate each trial and to provide a response. Five subjects (4 male, 1 female) were participants in the experiments testing dark cones explicitly, and one additional male subject was included in the normal cone psychophysical testing. All subjects (aged 22–51 years) had normal color vision (assessed by Hardy-Rand-Rittler plates and a Nagel anomaloscope) and no known retinal pathology based on comprehensive optometric eye exams. Luminance increment thresholds for the flashed microstimuli were measured using a Bayesian staircase method of threshold estimation.[34] Increment threshold was chosen as the test for light sensitivity because, at threshold, the stimulus is necessarily the least amount of light required to be perceived. Light levels representing threshold were converted to arbitrary units, ranging from 0 to 1, in order to control for day-to-day variations in stimulus intensity and allow comparisons between experiments. To provide a sense of the stimulus intensity in radiometric terms, we calculate that a typical 5 × 5 pixel stimulus (lasting ~130 μs) included ~12 log quanta at maximum intensity, presented on a background of ~8 log quanta incident at the cornea.[28] Two cones, one dark and a neighboring one with normal reflectivity to serve as a control, were targeted for stimulus delivery. All trials were randomly interleaved between each cone in a tested pair, and threshold was measured 3 to 5 times for each cone location (60–100 total trials) per experiment. Because of stimulus light level fluctuations, and also because threshold rises steeply with eccentricity, we analyzed the data with respect to relative threshold (between the two targeted cones) rather than raw threshold. Before any psychophysical data were used for analysis, subjects practiced the task to the point where reasonably consistent thresholds were obtained upon repeated measurements.

Ten cone pairs (one normally reflective and one poorly reflective) were monitored for both longitudinal imaging and psychophysical testing ($n = 5$ subjects). Six of these pairs were studied in one subject (age 23 years), with the remaining pairs in one subject each. Dark cones were initially selected as a cone-sized dark space within an otherwise normal cone mosaic. In three cases, the dark cone never increased appreciably in brightness. In seven cases, the cone occasionally reflected enough light to be visible; in these cases, the selected center was chosen based upon the cone's location on such imaging days. In cases where the dark cone was never visible, cone locations were estimated by choosing a point in the center of the cone-sized gap among neighboring cones. The 10 poorly reflective cones tracked longitudinally were tested only when they were darker than the field mean in the AOSLO image; this was required because some of these monitored cones occasionally exhibited normal reflectivity.

Investigative Ophthalmology & Visual Science

To validate the results obtained from the psychophysical testing of the dark/normal cone pairs, a larger population of normal cone pairs was also tested psychophysically. In these pairs, each of the cones in the pair exhibited normal reflectivity ($n = 56$ cone pairs, 6 subjects). These normal/normal cone pairs were tested in the same manner as described above.

Identification of Retinal Vessels

Retinal blood vessels and capillaries lying in front of the photoreceptors could, in principle, disrupt the light reflecting from the cones or interfere with stimulation light being delivered to the cones. In order to avoid these artifacts, vasculature maps were made for each targeted retinal location.[35] These maps were compiled using video processing tools to extract blood motion contrast cues from 30-second AOSLO videos taken with 710- or 840-nm light. By examining the vasculature maps that corresponded to the cone images at each site, we could select dark or normally reflective cones that were not associated with light path interference caused by retinal vessels.

Reflectance Quantification and Longitudinal Imaging

To obtain the AOSLO images used for reflectance quantification, two methods were used. First, for the majority of the cases, reflectivity data was obtained from images acquired during unrelated psychophysical experiments performed in the areas of interest. During each trial of a psychophysical experiment, a 1-second, retinally stabilized infrared video of 30 frames was recorded.[36] These frames were averaged after eliminating any blank frames or those with patent uncorrected eye-motion artifacts that are readily detected by automated image analysis. All single-trial average frames were then summed into one image, normalized to the brightest value, representing the cone reflectivity during one experiment. From these normalized images we quantified reflectivity for cones of interest. Second, if there were no prior psychophysical experiments performed in a selected retinal location, a 5-second retinally stabilized infrared video was taken (150 frames). These frames were also averaged to obtain a brightest-value normalized image (after manually removing frames with motion artifacts). Beyond the difference in total number of averaged frames, all cone reflectivity measurements were done in the same manner.

For the longitudinally monitored cone pairs, cone reflectance was quantified by first calculating the average pixel value for a 3×3 pixel square centered on each cone.[22] Dark cone locations were identified manually by choosing a point in the center of the cone-sized gap among neighboring cones (for persistently dark cones), or in the cone center if the cone was visible (for intermittently dark cones). For normally reflective cones, the center of the cone was chosen based on manual estimation of the pixel that was most centered within the cone (occasionally, this was not the brightest pixel). Because the mean reflectance value of an AOSLO image varies over time, we compared the mean pixel value of each cone to the mean pixel value of a 101×101 pixel field also centered on the cone. Reflectance was measured in standard deviations (SDs) from the field mean, to control for variations in image quality, laser power, and photomultiplier gain. Finally, for each of the 10 targeted dark/normal cone pairs, the same area of retina in each subject was repeatedly imaged over time to quantify cone reflectivity longitudinally (7–26 imaging sessions, representing 82–896 days).

To identify multiple cones within large fields, image processing was performed on normalized images using a custom local peak-finding routine (MATLAB; MathWorks, Natick, MA, USA). As this procedure did not always identify every cone correctly, especially those darker than the field mean, the processed images were surveyed manually and misidentified locations were corrected. In instances where cones were darkened due to interference by blood vessels and no peak was detected, cone locations were estimated based on local spacing. Individual cone reflectance was then quantified as described above.

Results

Imaging Characteristics of Poorly Reflective Cones

Images taken with AOSLO show considerable variation in reflectivity on a cone-by-cone basis. Examining five imaged fields of retina from five normal subjects, cones ranged in reflectance by a factor of 0.5 to 2.9 from the mean field reflectance ($n = 4{,}377$ cones from $\sim$169,000 μm^2 of retina), a range that is consistent with previous reports.[22,27,37,38] Some of the variation at the dark end of this range is likely to be associated with retinal blood vessels, which cover a substantial portion of the retinal surface.[39] To estimate what percentage of cones within an AOSLO image may be poorly reflective because of light path interference by retinal vessels, we compared the cone field to its overlying vasculature (Fig. 1). A map of the cones that had grayscale values below the mean image gray level was created (Fig. 1C) and then compared against the vascular map made at the same retinal location (Fig. 1D). As expected, most of the poorly reflective cones were associated with vessels. Of the 2,179 cones identified in the patch of retina shown in Figure 1, 346 cones (16%) had gray levels that fell below the image mean (red dots), while 1833 had gray levels at or above the image mean (black dots). However, a small number of these relatively dark cones were not obviously associated with vessels (blue circles). Such dark cones not associated with blood vessels were found in every subject (Fig. 2), in nearly every 1.2° field examined. Given their poor reflectivity, this subset of cones could represent either optical anomalies, present only at the time of imaging, or indicate possibly dysfunctional cones.

To learn if these unoccluded cones were only spuriously dark, we examined a longitudinal series of images to determine the persistence of the reflectivity. The reflectivity of 10 cone pairs, one dark and one normally reflective (depicted in Figs. 2D–M), was measured on multiple days. For each cone pair, there were 7 to 26 individual imaging sessions, over lengths of time spanning 82 to 896 days. Of these 10 dark cones, three never exhibited reflectivity that was higher than the mean image value (Figs. 2D–F), and were considered persistently dark. Figure 3A shows data for one cone that remained dark, despite neighboring cones that varied in brightness from day to day. The remaining seven cases occasionally exhibited reflectance that was higher than the mean field reflectance, thereby confirming the presence of a cone in these locations (often this required viewing images on a logarithmic grayscale to reveal the dim signal, as in Fig. 3). Data for one such intermittently dark cone is shown in Figure 3B, highlighting the fact that on most days, the cone was darker than the mean image reflectivity.

Psychophysical Testing of Poorly Reflective Cones

Because a small number of cones persisted in having anomalously low reflectance, we tested each of the 10

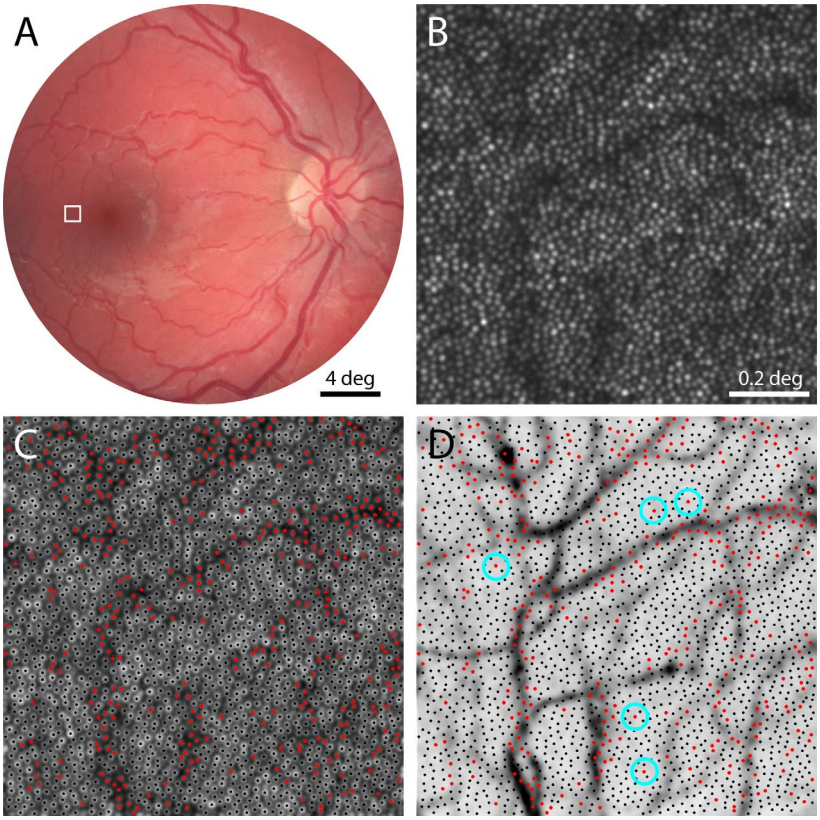

Figure 1. Relationship between poorly reflective cones and retinal vasculature. (**A**) Fundus photograph of the right eye of one subject. Outlined area shown magnified with AOSLO imaging in (**B**), where cone photoreceptors appear as bright spots (eccentricity = 2.7°). (**C**) Same field of view as in (**B**), with gray levels represented logarithmically to facilitate identification of poorly reflective cones. Cones brighter than the mean image reflectivity are marked with *black dots*, and those with reflectivity below the mean are indicated with *red dots*. (**D**) Vasculature map of same retinal area with cone centers from (**C**) superimposed, showing that most dark cones are associated with blood vessels. *Blue circles* mark dark cones that are not situated near blood vessels.

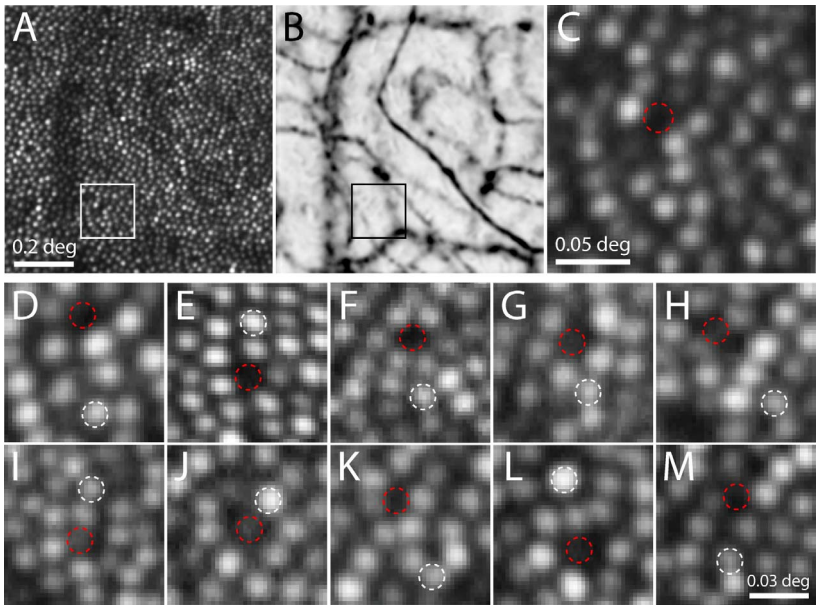

Figure 2. Identifying dark cones for longitudinal imaging and functional testing. AOSLO image (**A**) and vasculature map (**B**) from a second subject. Outlined area is magnified in (**C**), showing a dark gap in the cone mosaic where a cone could ordinarily fit (*dashed circle*), yet not situated under any blood vessels (eccentricity = 3.3°). (**D–M**) Images of 10 cone pairs on the day they were selected for threshold testing in 5 subjects (*white* = normal cone, *red* = dark cone). Persistently dark cones are shown in panels D–F, and intermittently dark cones in panels G–M. All of these sites were confirmed to not reside under blood vessels.

Investigative Ophthalmology & Visual Science

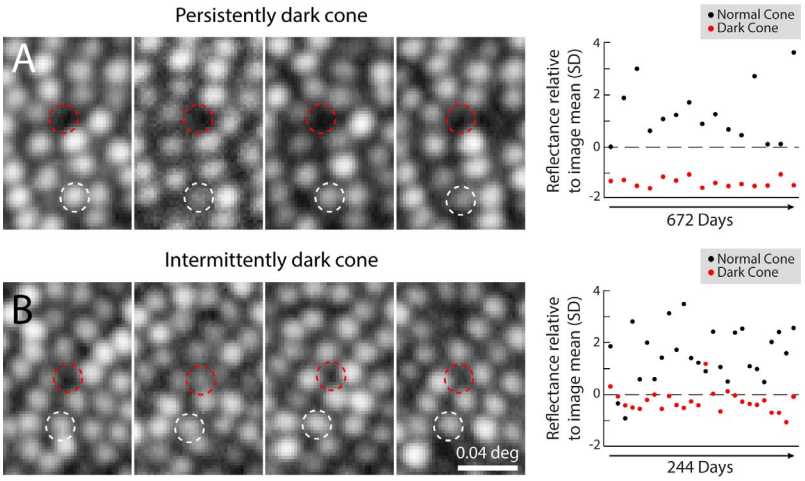

Figure 3. Poor cone reflectivity can be persistent or intermittent. (**A**) Longitudinal series of AOSLO images from a persistently dark cone in one subject, from the site illustrated in Figures 2A–C, shown on four separate imaging days (*left*). *Dashed circles* outline the same set of cones throughout (*white* = normal cone; *red* = dark cone), and indicate the locations where microstimulation was targeted for psychophysical testing. The normal cone varied in reflectivity, while the dark cone remained poorly reflective on all imaging days (*right*). (**B**) An intermittently dark cone, from the retinal area in Figure 1, is shown during 4 imaging days (*left*). In this case, the dark cone was intermittently visible (*second panel from left*), but did not vary as much as the normally reflective cone (*right*). All images in this figure are on a log intensity scale, to facilitate identification of relatively dark cones (note: this makes cone profiles appear larger; compare Fig. 2). Reflectance measurements were not taken at equal time intervals.

monitored dark cones psychophysically to determine if they were functional, using a staircase method to measure increment thresholds. All poorly reflective cones were tested for light sensitivity only when they were darker than the field mean in the AOSLO image. For the persistently dark cones, the stimulus was targeted at a manual estimate of where the cone center would be, given the position of neighboring cones (Fig. 4A). Testing one of the three persistently dark cases, the targeted dark cone location showed an increment threshold that was similar to the increment threshold obtained from its paired normally reflective cone (Fig. 4B). Data from one of the intermittently dark cones showed an increment threshold that was slightly lower than that of a nearby normally reflective cone (Fig. 4C). Because thresholds measured with such microstimuli can vary between cones for a number of reasons (discussed in Ref. 28), we compared the thresholds from the 10 dark cones to the 10 normally reflective cones as a population. To make this comparison, individual cone thresholds were normalized to the mean of each pairwise run of trials, to control for the effects of intersubject variability and visual field eccentricity on threshold. As a population, the dark cones did not have higher thresholds than the normally reflective cones that were tested at the same time ($P = 0.49$, Wilcoxon rank-sum test, Fig. 4D). Persistent and intermittently dark cones showed equivalent variation in threshold versus their paired normal cones.

To confirm that these thresholds were genuinely no different from normally reflective cones, we compared the dark/normal cone paired thresholds to a larger population of normally reflective cone pairs (56 cone pairs, six subjects). Threshold data were normalized as before; in addition, cone reflectivity was also normalized to the mean of each tested pair (Fig. 5). In this population of normally reflective cone pairs, the mean threshold was 3.6% higher in cones with less versus more reflectivity, a difference that was not significant ($P = 0.0502$, Wilcoxon rank-sum test). Had this correlation between cone reflectivity and threshold attained significance, it would still have been greatly outweighed by the ~80% variation in the thresholds observed in the normally reflective cone pairs. The targeted dark/normal cone pairs (Fig. 5, red points) exhibited the same variability in threshold and followed the same trend

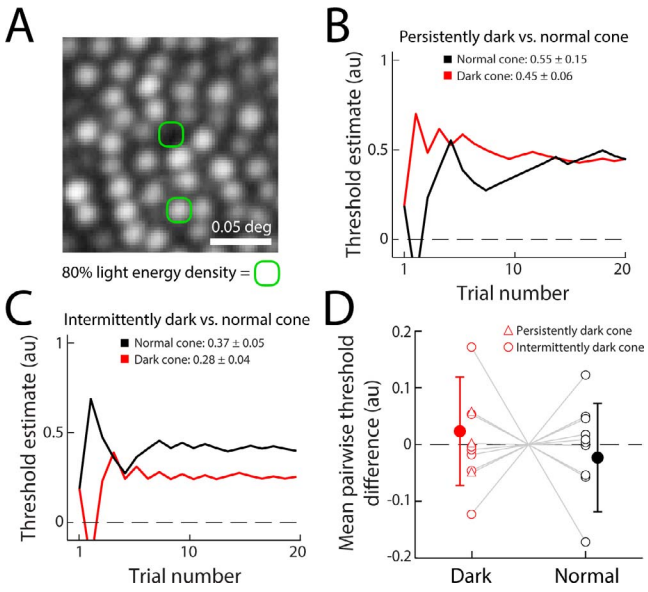

Figure 4. Microstimulation increment thresholds show no difference in light sensitivity between dark and normally reflective cones. (**A**) Schematic of the approximate size of the microstimuli. *Green* contour contains 80% of the integrated light energy delivered on the retina for a single stimulus flash. (**B**) Example staircase threshold estimates and mean values from repeated experiments for the persistently dark/normal cone pair shown in (**A**) and Figure 3A. Mean thresholds from three measurements (±1 SD) are indicated. (**C**) Example staircases for the intermittently dark/normal cone pair of Figure 3B, with mean thresholds from five experiments. Estimates in (**B**) and (**C**) are given in arbitrary units (au), spanning the range of deliverable light intensity. The threshold estimates are computed from the trial history. (**D**) Population mean threshold difference measured between 10 pairs of dark and normally reflective cones (filled data points). To compare thresholds across sites, each single-cone threshold was normalized to the mean of the cone pair thresholds for each run. Open data points represent the mean normalized thresholds computed from individual experiments. Dark and normal cone thresholds across the population did not differ significantly ($P = 0.49$; *error bars* ±1 SD).

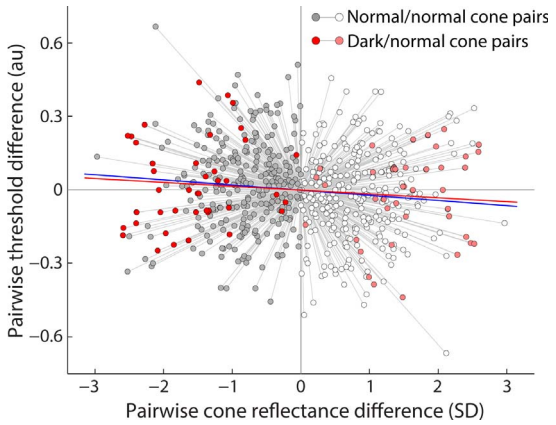

Figure 5. Comparison of single-cone reflectance and threshold. For both normal/normal (*grayscale*) and dark/normal (*red scale*) cone pairs, reflectance values for each cone were normalized to the mean reflectance of each pair during one experiment (indicated by *connecting gray lines*), expressed in SDs of the field gray level from the pairwise mean. Darker shading (*toward the left*) represents the less reflective cone in each pair. Cone thresholds were normalized to the mean of each cone pair, and plotted in arbitrary units from the pairwise mean. Linear regression reveals a 3.6% difference in mean threshold between normal cones with less versus more reflectivity (*blue line*, $P = 0.0502$, 284 paired threshold measurements). This trend was matched by dark/normal cone pairs, but also did not reach significance (*red line*, $P = 0.49$, 41 paired threshold measurements).

as the normally reflective cone pairs (Fig. 5, gray points). Also, as a population, there was no appreciable difference in absolute light levels for the dark/normal versus normal/normal pair thresholds, suggesting there was no local retinal effect on threshold. The range of reflectivity in these dark/normal cone pairs is on the extremes of the normal/normal cone pairs, as expected, since the inclusion of a dark cone increases the difference in reflectivity between cones in a pair.

Discussion

Our results suggest that cones that appear dark in AOSLO images and are not occluded by blood vessels remain normally sensitive to light, specifically when measured by luminance increment thresholds. One possible explanation for this is that residual scattered light from our stimulus is being detected by cones that surround the targeted cone. Light reaching these cones may arise from intraocular scatter or residual errors in our optical correction. In the case of normal intraocular scatter, experimental results and a model presented in Harmening et al.[28] showed that this does not play a detectable role in determining increment thresholds for cone-sized stimuli. Regarding imperfections in optical correction, in the diffraction-limited case, the resultant point spread function implies a very wide but very shallow intensity profile around the targeted cone. Less than 1% of the delivered light falls onto each of the six surrounding cones while more than 80% of the light lands within the targeted cone's inner segment profile.[28] Even if the optical correction was not completely diffraction-limited, this would likely raise the light delivered to surrounding cones by only a few percent. Thus, if the targeted dark cone was functionally compromised, and the neighboring cones were responsible for detecting the stimulus light, the measured increment threshold would still be greatly increased compared with the paired normally reflective control cone. Instead, the dark cones and paired normally reflective cones exhibited no difference in their observed thresholds (Fig. 4D), rendering it unlikely that neighboring cones could account for the increment thresholds measured from poorly reflective cones.

In the cases where the cones remained persistently dark, it might be hypothesized that the sites were actually small clusters of rod photoreceptors, which can occur occasionally at the eccentricities studied.[32] At present our AOSLOs cannot resolve rod photoreceptors, so they appear in the images as dark spaces surrounding the cones.[15,29] However, recent experiments have demonstrated that rod-filled gaps in the photoreceptor mosaic would not respond to the stimuli used here in the same manner as a cone photoreceptor would. On average, increment thresholds obtained from deliberately targeting microstimuli to the rod-sized gaps between cones was 48% higher than thresholds obtained when the stimuli were centered on a cone.[28] This result was accounted for by the cones outlining the gap. Moreover, the stimulus conditions here and in the gap-targeting experiments had background light levels that were rod-saturating, making any rod-mediated contribution to the task negligible. Therefore, our results are not likely to arise from any rod-mediated perception.

The question remains why a small set of cones with normal light sensitivity are poorly reflective on most days. Several independent factors may come into play. Waveguiding is one: small reflections that occur within the cone are efficiently directed back out of the eye because of the anatomical shape of the photoreceptors. This reflection is made more efficient because cones point toward the pupil due to phototropism.[21] Either waveguiding or cone pointing may be disrupted for these unusual cones. Given their waveguiding nature, a scanned beam directed at a cone may vary in reflection efficiency on short time scales because of interference between reflections within the cone.[26,28,37,40] This effect is partially mitigated by flood-illuminated systems, though cone reflectance still varies.[22,24,41] Because the cones we have examined are persistently dark, these interference effects cannot readily account for any lasting state of poor reflectivity. Instead, the cause is likely to be of anatomical origin.

Several possibilities exist. First, waveguiding may be inefficient because the cone may be dysmorphic. Without knowing more about the geometry of an occasionally misshaped cone, it is difficult to predict whether entering light will be proportional to reflected light, and therefore affect the relationship between threshold and reflectance systematically. Second, the reflections within a properly waveguiding cone may be reduced because the reflective interfaces within the cone (either between inner and outer segments or at the posterior tips of the outer segments) are permanently altered in some way. This anatomical anomaly would tend to separate the efficiency of light collection from light reflection. Finally, these uncommon dark cones may have aberrant orientations, pointing slightly away from the pupil rather than in the tightly aligned orientation most cones have.[22,42] All of these anatomical anomalies may persist over the time scales we have examined, and may be present in combination.

Regardless of the origin of the diminished reflectivity, it is not necessarily the case that a cone's reflectivity should positively correlate with its sensitivity. A cone that is weakly reflecting solely due to aberrant orientation will suffer a corresponding loss in light coupling and consequent sensitivity. However, there are factors working against this correspondence. One of the primary sources of reflection arises from the inner/outer segment junction,[22,25,43] and this reflection is light that has never passed through the cone's visual pigment. Second, most of the light coupled into a cone is either transmitted or absorbed. The portion that is reflected is on the order of 1% of what passes through the outer segments,[44] thus it may not be representative of the light that the cone detects.

Considering all this, it is unsurprising that cone threshold is not significantly influenced by large—and often short-term—changes in cone reflectivity (Fig. 5).

As mentioned earlier, the presence of dark cones in AOSLO images of many retinal diseases is not surprising, given the pathological changes that the tissue manifests. In some instances, dark cones in diseased retinas may not indicate photoreceptor death.[45,46] The possibility remains that dark cones in normal retinas cannot be considered homologues of dark cones in diseased retinas, so extrapolating functional tests from normal to diseased populations should not be done. In one study, a deuteranope with poorly reflective cones was found to have sensitivity deficits that suggested the mutation-affected cones were not functional,[20] whereas in another study examining a group of patients with retinal degenerations, functional tests appeared normal despite cone losses.[16] Thus, more work is needed to understand how each type of visual test (e.g., acuity, microstimulation) can be used to adequately characterize both normal and diseased retinas.

Because of its microscopic access to the photoreceptors, AOSLO imaging nonetheless has promise for becoming a powerful tool for early detection of disease and assessment of therapies. While many studies have examined the complex reflectance properties of cones, only recently has it been possible to probe cone function at the same microscopic scale. Cone-targeted microstimulation reveals that increment thresholds for individual cones vary considerably, even for adjacent cones when all other factors such as eccentricity and cone type are taken into account (Fig. 5). Such psychophysical data are consistent with the fact that the functional "weighting" of cones can vary when measured more directly in physiological experiments.[47–49] The use of microstimulation to assess function in a clinical setting, therefore, will have to take into account the wide variation in cone thresholds as well as cone reflectivity. The results shown here suggest that cones with diminished visibility in an otherwise normal-appearing retina do not necessarily indicate a sensitivity deficit. With a clearer functional picture of how a normal retina responds with AOSLO-based microstimulation, it can now be appreciated that cone thresholds vary widely. This variation will have to be taken into consideration when testing for nascent disease in patients with suspected retinal disorders but no macroscopic pathology.

Acknowledgments

We thank Andrew B. Metha and Christine A. Curcio for their manuscript comments.

Supported by Deutsche Forschungsgemeinschaft (DFG; Bonn, Germany) Ha 5323/3-1, Ha 5323/4-1, Ha 5323/5-1, NIH (Bethesda, MD, USA) T35HL07473, EY022412, American Optometric Foundation Ezell Fellowship (St. Louis, MO, USA), EY021642, EY014375, EY007043, EY023591, EY003039, EY023581, and the Eyesight Foundation of Alabama (Birmingham, AL, USA).

Disclosure: **K.S. Bruce**, None; **W.M. Harmening**, None; **B.R. Langston**, None; **W.S. Tuten**, None; **A. Roorda**, Canon USA, Inc. (P); **L.C. Sincich**, None

References

1. Carroll J, Kay DB, Scoles D, Dubra A, Lombardo M. Adaptive optics retinal imaging–clinical opportunities and challenges. *Curr Eye Res*. 2013;38:709–721.
2. Williams DR. Imaging single cells in the living retina. *Vision Res*. 2011;51:1379–1396.
3. Lombardo M, Parravano M, Lombardo G, et al. Adaptive optics imaging of parafoveal cones in type 1 diabetes. *Retina*. 2014; 34:546–557.
4. Choi SS, Zawadzki RJ, Lim MC, et al. Evidence of outer retinal changes in glaucoma patients as revealed by ultrahigh-resolution in vivo retinal imaging. *Br J Ophthalmol*. 2011;95: 131–141.
5. Chen Y, Ratnam K, Sundquist SM, et al. Cone photoreceptor abnormalities correlate with vision loss in patients with Stargardt disease. *Invest Ophthalmol Vis Sci*. 2011;52:3281–3292.
6. Hansen SO, Cooper RF, Dubra A, Carroll J, Weinberg DV. Selective cone photoreceptor injury in acute macular neuroretinopathy. *Retina*. 2013;33:1650–1658.
7. Stepien KE, Martinez WM, Dubis AM, et al. Subclinical photoreceptor disruption in response to severe head trauma. *Arch Ophthalmol*. 2012;130:400–402.
8. Syed R, Sundquist SM, Ratnam K, et al. High-resolution images of retinal structure in patients with choroideremia. *Invest Ophthalmol Vis Sci*. 2013;54:950–961.
9. Carroll J, Neitz M, Hofer H, Neitz J, Williams DR. Functional photoreceptor loss revealed with adaptive optics: an alternate cause of color blindness. *Proc Natl Acad Sci U S A*. 2004;101: 8461–8466.
10. Carroll J, Rossi EA, Porter J, et al. Deletion of the X-linked opsin gene array locus control region (LCR) results in disruption of the cone mosaic. *Vision Res*. 2010;50:1989–1999.
11. Choi SS, Zawadzki RJ, Keltner JL, Werner JS. Changes in cellular structures revealed by ultra-high resolution retinal imaging in optic neuropathies. *Invest Ophthalmol Vis Sci*. 2008;49:2103–2119.
12. Choi SS, Doble N, Hardy JL, et al. In vivo imaging of the photoreceptor mosaic in retinal dystrophies and correlations with visual function. *Invest Ophthalmol Vis Sci*. 2006;47: 2080–2092.
13. Duncan JL, Zhang Y, Gandhi J, et al. High-resolution imaging with adaptive optics in patients with inherited retinal degeneration. *Invest Ophthalmol Vis Sci*. 2007;48:3283–3291.
14. Roorda A, Zhang Y, Duncan JL. High-resolution in vivo imaging of the RPE mosaic in eyes with retinal disease. *Invest Ophthalmol Vis Sci*. 2007;48:2297–2303.
15. Merino D, Duncan JL, Tiruveedhula P, Roorda A. Observation of cone and rod photoreceptors in normal subjects and patients using a new generation adaptive optics scanning laser ophthalmoscope. *Biomed Opt Express*. 2011;2:2189–2201.
16. Ratnam K, Carroll J, Porco TC, Duncan JL, Roorda A. Relationship between foveal cone structure and clinical measures of visual function in patients with inherited retinal degenerations. *Invest Ophthalmol Vis Sci*. 2013;54:5836–5847.
17. Wolfing JI, Chung M, Carroll J, Roorda A, Williams DR. High-resolution retinal imaging of cone-rod dystrophy. *Ophthalmology*. 2006;113:1019. e1.
18. Talcott KE, Ratnam K, Sundquist SM, et al. Longitudinal study of cone photoreceptors during retinal degeneration and in response to ciliary neurotrophic factor treatment. *Invest Ophthalmol Vis Sci*. 2011;52:2219–2226.
19. Dubis AM, Cooper RF, Aboshiha J, et al. Genotype-dependent variability in residual cone structure in achromatopsia: toward developing metrics for assessing cone health. *Invest Ophthalmol Vis Sci*. 2014;55:7303–7311.
20. Makous W, Carroll J, Wolfing JI, et al. Retinal microscotomas revealed with adaptive-optics microflashes. *Invest Ophthalmol Vis Sci*. 2006;47:4160–4167.
21. Lakshminarayanan V, Enoch, JM. Biological Waveguides. In: Bass M, ed. *Handbook of Optics, Vol III: Vision and Vision Optics*. New York, NY: McGraw Hill; 2010:8.1–8.33.
22. Pallikaris A, Williams DR, Hofer H. The reflectance of single cones in the living human eye. *Invest Ophthalmol Vis Sci*. 2003;44:4580–4592.

23. Genead MA, Fishman GA, Rha J, et al. Photoreceptor structure and function in patients with congenital achromatopsia. *Invest Ophthalmol Vis Sci*. 2011;52:7298–7308.
24. Liang J, Williams DR, Miller DT. Supernormal vision and high-resolution retinal imaging through adaptive optics. *J Opt Soc Am A Opt Image Sci Vis*. 1997;14:2884–2892.
25. Jonnal RS, Rha J, Zhang Y, et al. In vivo functional imaging of human cone photoreceptors. *Opt Express*. 2007;15:16141–16160.
26. Bedggood P, Metha A. Optical imaging of human cone photoreceptors directly following the capture of light. *PLoS One*. 2013;8:e79251.
27. Roorda A, Romero-Borja F, Donnelly WJ III, et al. Adaptive optics scanning laser ophthalmoscopy. *Opt Express*. 2002;10:405–412.
28. Harmening WM, Tuten WS, Roorda A, Sincich LC. Mapping the perceptual grain of the human retina. *J Neurosci*. 2014;34:5667–5677.
29. Zhang Y, Poonja S, Roorda A. MEMS-based adaptive optics scanning laser ophthalmoscopy. Opt Lett. 2006;31:1268–1270.
30. Harmening WM, Tiruveedhula P, Roorda A, Sincich LC. Measurement and correction of transverse chromatic offsets for multi-wavelength retinal microscopy in the living eye. *Biomed Opt Express*. 2012;3:2066–2077.
31. Wyszecki G, Stiles, WS. *Color Science*. 2nd ed. New York, NY: John Wiley & Sons; 1982.
32. Curcio CA, Sloan KR, Kalina RE, Hendrickson AE. Human photoreceptor topography. *J Comp Neurol*. 1990;292:497–523.
33. Yang Q, Arathorn DW, Tiruveedhula P, Vogel CR, Roorda A. Design of an integrated hardware interface for AOSLO image capture and cone-targeted stimulus delivery. *Opt Express*. 2010;18:17841–17858.
34. King-Smith PE, Grigsby SS, Vingrys AJ, Benes SC, Supowit A. Efficient and unbiased modifications of the QUEST threshold method: theory, simulations, experimental evaluation and practical implementation. *Vision Res*. 1994;34:885–912.
35. Tam J, Martin JA, Roorda A. Noninvasive visualization and analysis of parafoveal capillaries in humans. *Invest Ophthalmol Vis Sci*. 2010;51:1691–1698.
36. Arathorn DW, Yang Q, Vogel CR, et al. Retinally stabilized cone-targeted stimulus delivery. *Opt Express*. 2007;15:13731–13744.
37. Putnam NM, Hammer DX, Zhang Y, Merino D, Roorda A. Modeling the foveal cone mosaic imaged with adaptive optics scanning laser ophthalmoscopy. *Opt Express*. 2010;18:24902–24916.
38. Rha J, Jonnal RS, Thorn KE, et al. Adaptive optics flood-illumination camera for high speed retinal imaging. *Opt Express*. 2006;14:4552–4569.
39. Snodderly DM, Weinhaus RS, Choi JC. Neural-vascular relationships in central retina of macaque monkeys (Macaca fascicularis). *J Neurosci*. 1992;12:1169–1193.
40. Jonnal RS, Kocaoglu OP, Zawadzki RJ, et al. The cellular origins of the outer retinal bands in optical coherence tomography images. *Invest Ophthalmol Vis Sci*. 2014;55:7904–7918.
41. Cooper RF, Dubis AM, Pavaskar A, et al. Spatial and temporal variation of rod photoreceptor reflectance in the human retina. *Biomed Opt Express*. 2011;2:2577–2589.
42. Roorda A, Williams DR. Optical fiber properties of individual human cones. *J Vis*. 2002;2:404–412.
43. Gao W, Cense B, Zhang Y, Jonnal RS, Miller DT. Measuring retinal contributions to the optical Stiles-Crawford effect with optical coherence tomography. *Opt Express*. 2008;16:6486–6501.
44. Berendschot TT, DeLint PJ, van Norren D. Fundus reflectance–historical and present ideas. *Prog Retin Eye Res*. 2003;22:171–200.
45. Wang Q, Tuten WS, Lujan BJ, et al. Adaptive optics microperimetry and OCT images show preserved function and recovery of cone visibility in macular telangiectasia type 2 retinal lesions. *Invest Ophthalmol Vis Sci*. 2015;56:778–786.
46. Jacob J, Paques M, Krivosic V, et al. Meaning of visualizing retinal cone mosaic on adaptive optics images. *Am J Ophthalmol*. 2015;159:118–123.
47. Sincich LC, Zhang Y, Tiruveedhula P, Horton JC, Roorda A. Resolving single cone inputs to visual receptive fields. *Nat Neurosci*. 2009;12:967–969.
48. Field GD, Gauthier JL, Sher A, et al. Functional connectivity in the retina at the resolution of photoreceptors. *Nature*. 2010;467:673–677.
49. Li PH, Field GD, Greschner M, et al. Retinal representation of the elementary visual signal. *Neuron*. 2014;81:130–139.

Investigative Ophthalmology & Visual Science